

A feasibility study on semi industrial nozzleless electrospinning of cellulose nanofiber

Iman Esmaeilzadeh¹ · Vahid Mottaghitalab¹ · Behnam Tousifar¹ · Arezoo Afzali¹ · Mastooreh Lamani¹

Received: 9 March 2015 / Accepted: 1 July 2015 / Published online: 17 July 2015
© The Author(s) 2015. This article is published with open access at Springerlink.com

Abstract The current study focuses on the production of cellulose nanofiber through semi-industrial nozzleless electrospinning process. The cellulose biopolymer used for spinning process was extracted from rice straw as renewable, abundant, and inexpensive natural resource. The electrospinning device comprising one needle is extremely inefficient because of low productivity level of about 0.3 g/h. Thus, using the nozzleless electrospinning system guarantees the high productivity of nanofiber web for diverse applications. The successful electrospinning process is accomplished through systematic control of the surface tension, viscosity, and electric conductivity of aqueous solutions of cellulose. Moreover, a design expert software was used for providing experimental plan for the investigation of the influence of the operational conditions on the spinning properties of the selected solution. The polyvinyl alcohol with a weight ratio of 60 % relative to cellulose content was used as a biocompatible polymer to facilitate electrospinning process for producing the aqueous cellulose solution of 0.63 wt%. Based on the scanning electron microscopy images, and various selected parameters, namely, the drum rotation rate of 9 rpm, high voltage range of ± 55 kV, the spinning temperature of 41 °C, and 10-cm distance between drum and collector an average diameter of 89 ± 1 nm was arrived. The composite nanofibers used for filter production and their performance were

evaluated by porosity analysis and permeability tests. Results show the negative impact of the weak mechanical strength as an obstacle in Penetration test. (It promotes by higher electrospinning time and reaching proper stiffness in web layer.) The permeability tests show a maximum value of $3.5 \text{ cm}^3/\text{cm}^2/\text{s}$ at the maximum pressure of 120 Pa.

Keywords Cellulose nanofiber · Needle less electrospinning · Rice straw · Filter

Introduction

The oil resources forms more than 50 % of the raw material required for synthetic fiber production. This level of oil consumption is extremely challenging because of the limited sources of fossil-based hydrocarbons. Using cellulose resource either wooden or non-wooden material in fiber related industry attracted the attention of green material researchers in recent years [1, 2]. The non-wooden plant is the predominant source of highly pure cellulose used for producing diverse micro to nanostructure materials including film, paper, non-woven mat, and fiber [3, 4].

The most essential non-wooden cellulosic material such as corn [5], wheat [6], rice [7], and soybean [8] are very well known for the usefulness of their straws in diverse applications.

These materials, in fact, provide roughly 2200 million tons of by-products. The reusing of 10 % of prescribed byproducts is enough to produce more than 40 million ton fibers even if only 20 % w/w of byproducts were efficient. This remarkable amount is equivalent to about 57 % of annual fiber production which is nearly 70 million tons [9, 10].

✉ Vahid Mottaghitalab
mottaghitalab@guilan.ac.ir

¹ Textile Engineering Department, Faculty of Engineering, University of Guilan, P.O. Box 3756, Rasht, Iran



Cellulose is the most abundant polymer available worldwide and its unique properties such as biocompatibility, mechanical strength, specific microfibrillar morphology, and chemical structure make it as a promising and potentially the most important substituted natural candidate material for polymer industry. Cellulose molecular structure is extremely strong as a pile of nanoscale crystalline region [11, 12]. It is a linear homopolysaccharide composed of D-glucopyranose units linked together by β -1,4-glycosidic bonds. Fibril structure of α -cellulose with high crystallinity plays a substantial role to contribute to the mechanical resistance in cell walls. Also, the presence of intermolecular and intramolecular hydrogen bonds leads to higher chemical and mechanical resistance properties [13]. Figure 1 shows the cellulose chemical structure with closed chemical formula of $C_{6n}H_{10n+2}O_{5n+1}$ (n represents the polymerization degree).

Among many countries, the straw byproducts from cultivation fields of grains like wheat, rice, corn, and soybean can be considered as an important lignocellulosic resources consists of lignin, hemicellulose, and cellulose [14]. Their quantity depends on type of plant, methods of growing, humidity, and geographic conditions. It was reported that the cellulose contents of wheat straw, rice, black wheat, barley, oat, bagasse, corn stalks, and maize, respectively, are 38.6, 36.5, 37.9, 34.8, 38.5, 39.2, and 43.2 % w/w. The quantities of cellulose, hemicellulose, and lignin for a variety of cellulosic material were reported in the previously published literature [15, 16]. Rice straw, however, consists of 32–47 % w/w cellulose, 19–27 % w/w hemicellulose, and 5–24 % w/w lignin [17, 18]. Thus, it can be stated that the cellulose derived from rice straw is dramatically more valuable if it passes the extraction process efficiency test [19].

Geometric specifications of nanocellulosic structures including shape, length, and diameter depend on cellulose resource and the production method [20]. In the meantime, nanocellulose can be separated into three categories: crystalline nanocellulose, cellulosic nanofiber, and nanocellulosic composites [21]. Among them, cellulosic nanofibers are the most significant product because of its unique properties like higher surface area-to-volume ratio, greater mechanical strength, a lower thermal conductivity, and higher porosity. Compared to other commercialized

techniques, electrospinning process involves a novel and efficient method for nanofiber production. This small diameter, for example, leads to a high area-to-mass ratio of $10 \text{ m}^2/\text{g}$ for diameters of about 500 nm. This value reaches to $1000 \text{ m}^2/\text{g}$ for diameters close to 50 nm. Moreover, access to the lower diameter allows obtaining a huge surface area-to-volume ratio of roughly more than 1000 times compared to microfiber. The continuous formation of nanofiber is another advantageous characteristic of electrospun nanofiber compared to other forms of cellulose nanostructure.

In electrospinning process, a strong electric field is applied on a droplet of polymer solution (or melt) held by its surface tension at the tip of a syringe's needle (or a capillary tube). As a result, the pendent drop becomes highly electrified, and the induced charges are distributed over its surface. Upon increasing the intensity of electric field, the surface of the liquid drop will be distorted to a conical shape known as the Taylor cone. Once the electric field strength exceeds a threshold value, the repulsive electric force dominates the surface tension of the liquid, and a stable jet emerges from the cone tip. The charged jet is then accelerated toward the target, and the jet rapidly thins and dries because of elongation and solvent evaporation. As the jet diameter decreases, the surface charge density increases, and the resulting high repulsive forces splits the jet to form smaller jets. This phenomenon may take place several times leading to a large number of small jets. Ultimately, solidification occurs, and fibers are deposited on the surface of the collector as a randomly oriented nonwoven mat [22]. The main step to make a feasible electrospinning process is based on the selection of proper solvent for forming a solution with optimal surface tension, conductivity, and viscosity.

In addition, the chemical nature of cellulose because of its powerful hydrogen and van der Waals bonds on its molecular structure prohibits its solubility in common organic or aquatic solvent. However, many solvents were reported in the literature for facile solubility of cellulose including Formic acid/Zinc chloride [23], aquatic mineral complexes such as cuen, cadoxen, cuoxam [15], 10 % Caustic soda aquatic solution, mineral acids, mixture of hydrated salt minerals, *N,N*-dimethylacetamide/Lithium chloride, dimethyl sulfoxide, three ethylamine/Ammonium sulfur dioxide, *N,N*-dimethyl formaldehyde/ N_2O_4 , and dimethyl sulfoxide/para formaldehyde [24, 25]. Our recent study on spinnability of rice straw showed that the low volatility, toxicity, and high cost are listed as most common disadvantages of some of the solvent systems [26]. Therefore, ever-increasing attentions have been paid to introduce ecofriendly solvent to use cellulose biopolymer in a variety of applications. For instance, Jia and his co-

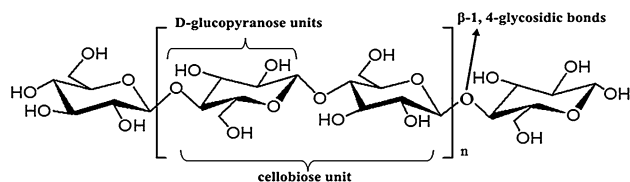


Fig. 1 Chemical structure of cellulosic chain



workers [27] used water as a solvent for preparation of electrospinning solution from polyquaternium-4 cellulose (PQ-4).

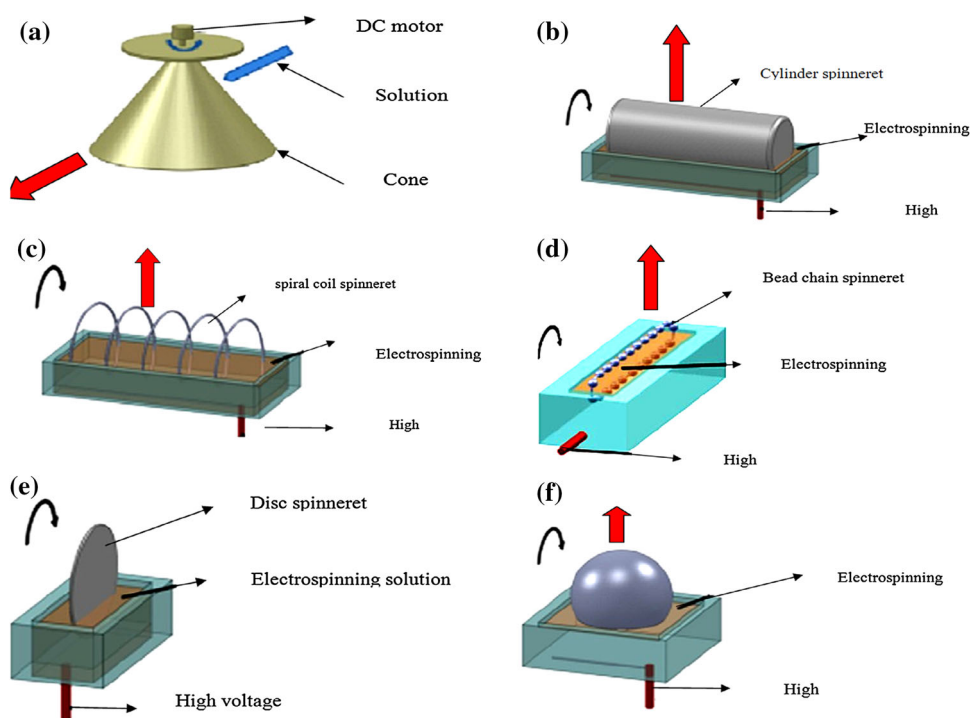
Most of the electrospinning processes on cellulose and its derivatives were carried out by using a needle-and-syringe pump system. Even then, the little output of fluid in single-needle electrospinning restricts the production capacity on industrial scale, which is mainly less than 0.3 g/h [28, 29]. There are several suggestions for the improvement in the electrospinning production rate [30].

The effort to scale up the electrospinning technology to attain an industrial level of production followed by multiplication of the jets using multinozzle construction. However, the number of jets needed to reach economically feasible productivity is very high, typically on the order of thousands. This brings into play many challenging tasks, generally related to reliability, quality consistency, and machine maintenance (especially cleaning). The nozzleless electrospinning solves most of these problems due to its mechanical simplicity; however, the process, itself is more complex because of its inherent multi-jet nature [31].

Recently, nozzleless electrospinning devices were reported for raising the production rate of nanofibers [32]. The nozzleless electrospinning forms nanofibers directly from the exposed surface of fluid. There are many jets, which are simultaneously produced from the nozzleless spinneret. Figure 2 schematically shows the various types of nozzleless spinneret for making thousands of fluid

threads move toward the collector plate. The formation of primary jet in nozzleless electrospinning leads to the self-orientation which happens on the fluid's exposed surface. The control of spinning process is difficult, and the spinnerets play a basic role in needleless electrospinning process including assuring fiber quality and high efficiency [33]. The nozzleless electrospinning was introduced for the first time in 1970 by Simm and his coworkers, which used one disk for electrostatic spin fiber that is utilized in filtration [34]. It was followed by Jirsak group who commercialized nozzleless electrospinning system with a cylinder or a roller for producing fibers (spinneret) by their group company, Elmarco, in the brand name of Nanospider [35]. Niu and his coworkers used a disk as a spinneret for producing of nanofibers [36]. Yarin and Zussman used magnetic fluid beneath a polymeric solution for the initiation of needleless electrospinning [37]. Liu and his colleagues exploited air bubbles to produce nanofibers in electrospinning from a fluid surface [38]. The commercial nozzleless electrospinning process is currently widespread in the world, and most of companies utilize this technique for mass production of nanofibers [39]. Different kinds of spinning spinnerets with the ability of rotating in a polymeric solution bath transfer the solution toward collector plate. This stimulation can be conducive for the establishment of primary Taylor cone during electrospinning. Formation of jets in needleless electrospinning can be divided into four sections. First, a thin layer of polymeric solution formed on

Fig. 2 The schematic representation of spinning spinneret for nozzleless electrospinning process



the surface of spinneret results in plunging and spinning of the solution. Then, spinning of spinneret also causes turbulence and stimulation of the formed solution's layer on the spinneret, and as a consequence, primary cones are established on the surface of solution. Afterward, when the high voltage is applied, the concentration of electrical power on cones on the surface of solution causes enhanced turbulence. Finally, the stretched jets emerge from Taylor cone, and nanofibers are formed on the moving collector plates [33]. The spinning module can create continuous primary mechanical vibration in polymeric solution, and the creation of turbulence in polymeric solution helps in some way to produce primary jets [33].

The cellulosic nanofiber is employed in a variety of applications in different areas including optical [40], electronic [41], medical [42] engineering, and membrane technology [43]. One of the extremely important applications of nanofibers has been proposed for filtration technology which extensively increases the efficiency and dramatically reduce the pressure drop during the separation process [44, 45]. The filter performance is mostly influenced by the diameter and the corresponding porosity since the size of particles or that of droplets needs to make them impermeable to membrane media according to nanoscale porous web of fibers [46]. The membrane's utilization as nanofiber in different areas is found to be of 70 % of all the patented documents so far [47].

In the current study, the extracted cellulose in aqueous solution derived from rice straw was used as a primary natural biopolymer for producing cellulose nanofiber using nozzleless electrospinning process. The cellulose nanofibers were produced to explore the air permeable and porous nanofiber web for further application in the membrane industry.

Experimental

Chemical and reagents

The extracted cellulose from rice straw was purchased from Aria Cellulose Company (GSTP, IRAN) and used without further purification. The ionized water as a pure solvent was used for preparation of aqueous solution of cellulose. The anionic surfactant of sodium dodecylbenzene sulfonate and lithium chloride supplied by Sigma Aldrich were used without further treatment. Further softening process was carried out using glycerin. Also, the polyvinyl alcohol (PVA) with molecular weight of 72,000 g/mol made by MERK Company was used as secondary polymer.

Preparation of aqueous spinning solution of cellulose

The polymeric electrospinning solutions with various cellulose contents of 0.63, 0.9, 1, 1.25, and 1.5 % w/w were prepared using ionized water. The particle-free and the homogenous solution was prepared using magnetic stirrer for 24 h at the room temperature. In the next step, the sufficient amounts of surfactant and the lithium salt were so selected to obtain minimum surface tension, higher conductivity, and enough viscosity. The electrospinning process facilitates using a 10 % w/w of PVA aqueous solution, which is vigorously mixed under stirring for 24 h using a magnetic stirrer in cellulose/surfactant/lithium salt solution with the ratio of 40/60. The cellulose and PVA composite spinning solution mixture was stirred for 24 h at room temperature using the magnetic blender.

Characterization of spinning solution parameters

The characterizations of spinning parameters are essential since the successful electrospinning process needs a proper polymeric solution. The measurement of liquid surface tension was carried out by weight measurement technique. The equipment includes a digital pump to control the output speed of polymeric solution, a syringe as a solution-holding container, a needle with a specific inner diameter, and an accurate balance for output solution measurement. The surface tension measurement was accomplished based on Tate's law [48]. The Brookfield-RV-DV II+ viscometer was used to determine the rheological properties of spinning solution and Orion conductivity meter Model 140 was used to measure solution conductivity.

Electrospinning process

The electrospinning in semi-industrial scale manufactured by FNM (CO, LTD, IRAN) was used in the current study for preparation of continuous cellulose nanofiber web. The laboratory electrospinning device has needle as a spinneret. However, disk or cylinder is used in nozzleless electrospinning process. Cellulosic spinning solution is poured into the spinning bath in which the cylindrical or spiral spinneret rotates. Due to spinneret's rotation, the solution stick loosely on the spinneret's surface and moves toward top point. The applied voltage between spinneret and collector forms numerous Taylor cones as a convergent fluid flow for travel in the spinning line toward the collector. The alterations in the electrospinning parameters enable production of nanofibers with a variety of specifications. The images of the electrospinning pilot plant equipped with three spinning baths used in this research are shown in Fig. 3a, b. The current apparatus used in this study is an upward electrospinning system, implying that the collector



Fig. 3 **a** General views of nozzleless semi-industrial electrospinning frame. **b** Internal view of nozzleless electrospinning frame

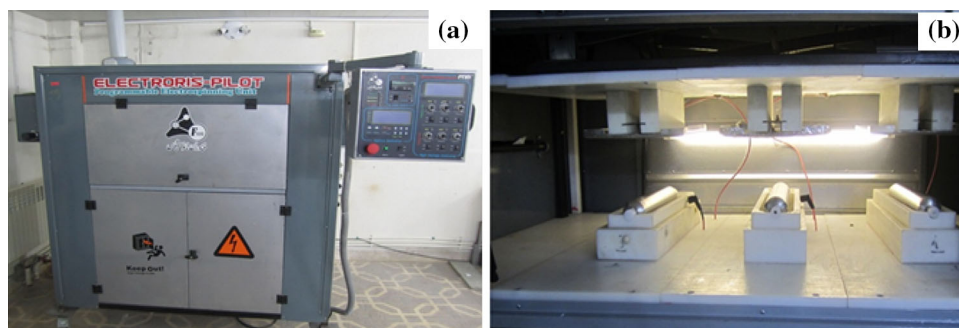
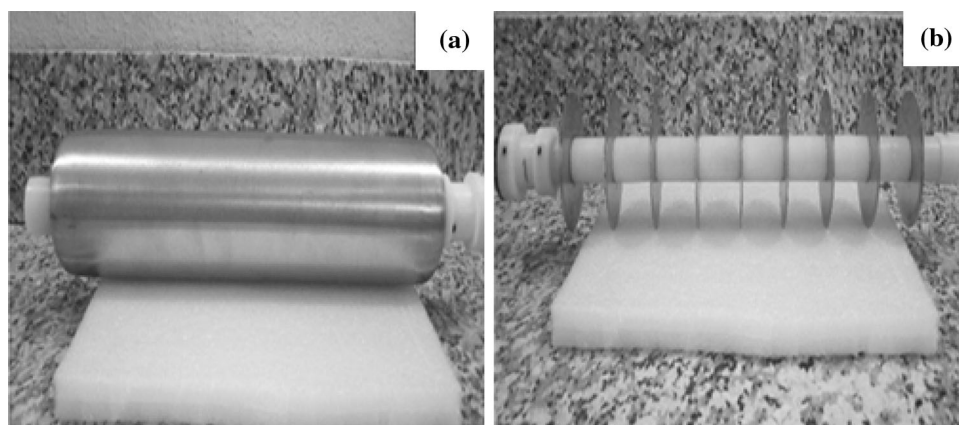


Fig. 4 **a** Cylindrical and **b** disk spinnerets



is placed above the spinneret, including three storage baths of polymeric solution for improving the production rate. Spinning solutions are stored in the baths that are connected to positive voltage terminal through a metal nut at the bottom of the bath plate leading to solution charging. Figure 4 shows the storage bath of the spinning solution and the linking terminals of positive electrode.

The collector is also connected to negative voltage terminal by a wire to create an essential electrical field during the electrospinning process between the spinneret and the collector. The two kinds of spinneret, having cylindrical or disk shape, were used for producing the nanofibers (Fig. 4). Disk spinneret has nine disks on the same axis to raise the system output. Cylindrical spinneret has 35 cm length and 6 cm diameter. Although disk spinneret has the same diameter, it has 0.5-mm thickness with the inclined edges. The gap between disks is 4 cm, and the rotating speed varies from 0.5 to 9 rpm. The spinning solution level should not be less than half of the total bath volume. The lower level of solution should be as high as layer thickness of solution on the spinneret and increase the possibility of electrical discharge during electrospinning. The phrase “distance in nozzleless electrospinning” means the distance between the spinneret’s surface and the collector plate. In this framework, there is no chance to independently alter the distances between spinneret and collector

for each bath. Electrospinning device possesses a substrate system which is able to move in both left and right directions. The paper, fiber, or other kinds of substrates can be used as guide material. There are two rollers in the two sides of the apparatus frame: one for feeding and the other for collecting the substrates. For each of bath, however, it is possible to control the voltage value by means of the control panel of device. It is possible to electrospin all the three polymeric solutions simultaneously by applying different voltages. The voltage range for either positive or negative voltages can be adjusted between 1 and 60 kV. Therefore, every bath ultimately works under summation of negative and positive voltage equal to 120 kV. For safety purposes and inhibiting the electrical discharge, applying less than 35 kV to either positive or negative voltage is strongly recommended. Also applying more than 50 kV as the sum of voltages between the negative and positive electrodes, when the distance between the collector and the bath is less than 10 cm is absolutely prohibited. The temperature variation is also a sophisticated technique for process control achieved through decreasing the surface tension. Two embedded heaters are placed in two sides, which are able to increase the temperature to around 50 °C inside the electrospinning box. The release of toxic and hazardous gases during the electrospinning process is prevented by the air conditioning system assembled to the



left side of the spinning box. This system removes toxic and hazardous gases from the working area. The optimal spinning solution can be selected based on the electrospinning solution parameters (surface tension, conductivity, and viscosity. Table 1 lists the parameters with their ranges and units for further consideration.

The experimental design based on response surface methodology was utilized to determine optimal amount of affecting data. Although many factors and connections have a remarkable influence on the response variable, superficial analysis of response is one of the effective ways to determine several variables with least data, resources and designing efficient experiment. The central composite protocol is used in a specified range with the least performance by distributing experimental points for model curve fitting. Hence, based on the three variable parameters including spinneret rate, voltage, and gap, a total number of 20 experiments are developed with three levels and six repetitions in the central point of the design. Table 2 shows the specifications and details of each experimental lot.

Table 1 Ranges of electrospinning parameters for DE7 software

Factor	Parameters	Unit	Minimum	Maximum
A	Speed of spinneret	rpm	1	9
B	Applied voltage	kV	30	80
C	Spinneret and collector gap	cm	5	12

Characterization techniques

Optical microscope

The polarized optical microscope (Nikon, Japan) with 100× magnification and sample holder was utilized for the formation of nanofiber. The presence of collected nanofiber on glassy slide was observed using an optical lens.

Scanning electron microscope

The morphology of the nanofibers was observed for different magnifications using a scanning electron microscope (Philips, XL30, Netherland) at an acceleration voltage of 17 kV. Materials were sputter coated with gold prior to imaging. Fourier transform infrared (FTIR) (Nicolet, 560, USA) spectroscopy was used to examine the structural changes of the rice straw, which occurred after each treatment.

Fourier transform spectroscopy

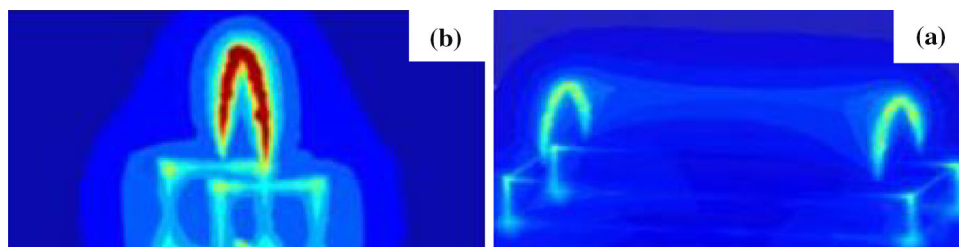
Fourier transform infrared (FTIR) spectra were recorded using a Nicolet 560 spectrometer to investigate the conformation and the crystallinity of nanofibers in the wavelength range of 500–4000 cm^{-1} under an absorbance mode.

Table 2 Experimental design for electrospinning parameter

Experiment	Speed spinneret (rpm)	Voltage (kV)	Spinneret distance to collector (cm)
1	5	55	5
2	1	55	8.5
3	9	80	12
4	5	80	8.5
5	5	55	8.5
6	9	55	8.5
7	9	80	5
8	1	30	12
9	5	55	8.5
10	5	55	8.5
11	5	55	8.5
12	9	30	5
13	9	30	12
14	1	30	5
15	5	30	8.5
16	5	55	12
17	5	55	8.5
18	1	80	12
19	1	80	5
20	5	55	8.5



Fig. 5 Curves of electric fields' intensities of **a** cylindrical and **b** disk spinnerets



Permeability test

Air permeability can be recalled as the volume of air passing a definite surface under a specific external pressure. The Air permeability tester FX 330 was utilized to measure the permeability value. The web porosity can be referred as the most influential parameter in affecting the air permeability specifically at various air pressures and as an extremely critical and effective parameter. The instrument utilizes a tube with inside area of 5 cm^2 and a sample holder to fix the position, while the suction proceeds. The unit of measurement for the permeability test based on transmitted air through specific cross-sectional area per unit time is designated as $\text{cm}^3/\text{cm}^2/\text{s}$.

The analysis of fiber diameter and porosity

The diameter measurement in nanoscale can be carried out using SEM pictures and image J processing software. The picture in jpeg or tiff format is recognized by software in first step. Then, the adjusted scale is defined based on the picture scale bar. Finally, several measurements of diameter from the entire surface, say around 100, need to be made, and the results include the average value and its distribution.

The porosity also can be measured by a sophisticated technique which is developed based on the a program in MATLAB compiler [49]. According to the principle of methodology, first the images are brought up in gray scale mode, and then based on the threshold value, the binary pictures are created with different levels. The threshold value determines the depth level in binary pictures. Based on various threshold levels, three surface levels are evaluated, and the average value of these three layers is reported as the porosity value of the whole layer [50].

Results and discussion

Figure 5 shows the contour plot of electric field intensity for two cylindrical and disk spinnerets. As can be seen, higher intensity of electric field is usually formed on the extremity of the cylinder, and the lower one is formed in the middle of surface. On the other hand, for the disk

spinneret, higher intensity of electric field is almost formed around edges, and its strength is higher than cylindrical nozzles.

Because of the high crystallinity and hydrogen bonds, there is less possibility for the cellulosic polymer to dissolve in usual solvent, and a special equipment is needed for quicker evaporation and a supplementary material needed to reduce the fluid viscosity. Despite introducing different solvent systems for producing cellulosic nanofibers, there are some kinds of problems such as spiraling costs, toxicities of materials, and dependence on coagulating bath during electrospinning process. The current study tried to apply biocompatible solvent, and environmental-friendly, inexpensive. and accessible supplementary material. Moreover, the analysis was carried out by the possibility of producing cellulosic nanofiber derived from rice straw. In addition, the optimal condition for producing cellulosic nanofiber and its corresponding physical and chemical properties were obtained based on spectroscopic and microscopic data.

The characterization of cellulose solution

The aqueous solutions were produced with the cellulose contents of 0.63, 0.9, 1, 1.25, and 1.5 wt%. The surface tension, conductivity and viscosity were measured for selecting the best solution. As is shown later, transparent and particle-free solutions are prepared by gentle agitation of cellulosic polymer in water (Fig. 6).

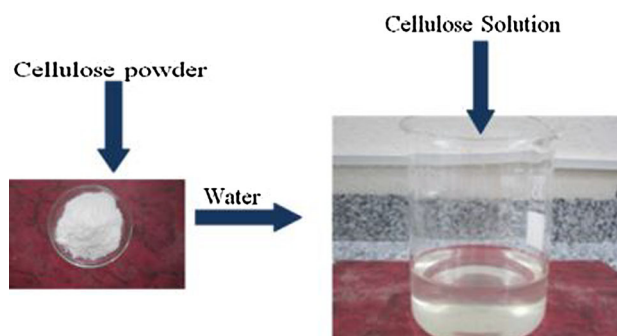


Fig. 6 The transparent cellulosic solutions prepared from rice straw-extracted cellulose



Table 3 Surface tension, conductivity, and viscosity data for cellulosic solutions

Surface tension (mN/m)	Conductivity (mS)	Viscosity (cP)	Concentration (% w/w)
55.5	1.73	148	0.63
62	1.24	514	0.9
63	1.28	1033	1
75	1.48	2241	1.25
82	1.49	4007	1.5

Table 4 Results of adding Lithium Chloride salt into cellulose/water solution

Surface tension (mN/m)	Conductivity (ms)	Cellulose concentration (% w/w)
55.5	1.73	0.63 % w/w
54	23	0.63 % with 1 % lithium chloride
54	34.6	0.63 % with 2 % lithium chloride
57	56.6	0.63 % with 4 % lithium chloride

The results obtained from surface tension, conductivity, and viscosity tests for cellulosic solutions are shown in Table 3.

Surface tension is one of the most important parameters in the ejection of jets from the surface of polymeric solution. The lower the surface tension of the spinning solution, the stronger the force that prohibits spinning jet formation. After producing spinning solutions, it was specified that the 0.63 % w/w cellulose solution has less surface tension compared to the other spinning solution. The surface tension increases with the increasing cellulosic concentration. Results show negligible conductivity variation with changes in the cellulose content. In addition, the viscosity is an extremely influential parameter on electrospinning process which plays a vital role in determining the size and morphology of nanofibers during fiber spinning. The low viscosity causes inability to form continuous nanofibers; on the other hand, high viscosity causes hindrance to the ejection of jets from the spinneret surface. Hence, the viscosity optimization is critically important for efficient electrospinning [51]. Suitable viscosity for electrospinning solutions would be from 100 to 400 cp [52]. With the increasing cellulose concentration, the viscosity of cellulosic solution increases based on a quadratic (second-degree equation) model. According to these results, solution with 0.63 % w/w shows proper behavior for electrospinning compared to other solutions. However, the high surface tension and low conductivity make a powerful barrier against fiber jet formation. Hence, another strategy followed by adding Lithium chloride salt into cellulose/water solution.

It was observed that the conductivity of solution in the absence of salt is fairly low, while the conductivity is one of the most prominent parameters in electrospinning. The lowest voltage in the formation of Taylor cone will decrease with the increasing solution conductivity [53].

Increase of the amount of the lithium chloride is effective by using two capable methods: the first one is that the ion increases by the salt concentration, and consequently, surface charge density increases in fluid surface. Also motive electrostatic power on the surface of fluid increases by external electric field [53]. Different amounts of the lithium chloride were added to 0.63 w/w % cellulosic solutions, and their influences were observed on other solution parameters. The results show the monotonic increase of the conductivity with additions of 1, 2, and 4 % w/w of salt in the selected solution. Yet, there is no noticeable change in the surface tension, and its range of variations is not considerable. The conductivity is adjusted to prevent uncontrolled spraying during electrospinning. Taking into consideration all these factors, 0.63 % w/w solution with 1 % w/w salt was found to be more efficient, which was, therefore, selected for further experiments [53].

Data given in Table 4 make an attempt to explore the effects of salt addition on conductivity and surface tension. It has been shown that the addition of salt has little effect on surface tension, and mostly increases the conductivity. Moreover, our observation revealed that the addition of salt demonstrates negligible effect on viscosity.

As can be seen, the surface tension of the as-prepared solutions is out of range, and the capability of electrospinning is reduced depending on the failure in overcoming surface tension. A decrease in surface tension can be proposed by the addition of anionic surfactant to cellulose/water solution. A remarkable decrease in surface tension was observed from 54 mN/m to 44.4 after addition of anionic surfactant powder to the 0.63 % w/w polymeric solution of cellulose. Therefore, the inclusion of anionic surfactant to the selected cellulose solution causes noticeable decrease in surface tension. Conductivity remained unchanged, and as a result, it can be expressed that the surfactant has no significant influence on conductivity, but



its viscosity increases compared to surfactant-free solution to a value of about 345 cP. It can be seen, the viscosity is still in the efficient range of 100–400 cp for electrospinning. It is worthy to note that the selecting efficient density of cellulose and optimal amounts of Lithium Chloride and anionic surfactant leads to the best viscosity, conductivity, and surface tension. Hence, the solution containing 0.63 % w/w solution with 1 % Lithium Chloride salt and 10 mg anionic surfactant were selected as the most suitable solution for electrospinning.

Cellulosic nanofibers from cellulose/water/surfactant/salt solution

Electrospinning with nozzleless electrospinning apparatus was carried out based on designated experimental plan as shown in Table 2. Spinning parameters including voltage, speed, and distance were adjusted to make each sample on a glassy slide attached onto the collector. The collected nanofibers were precisely studied with the optical microscopy. The higher the temperature, the less the surface tension that is obtained. However, the highest temperature attainable by the system is induced by high thermal power devices. The disk spinneret was used because of its higher field power compared to cylindrical spinneret. The response variable and its scales for each set of experiment were defined between 0 and 10, respectively, for both the droplet and the dense and uniform nanofiber distribution. Then influences of spinning parameters were analyzed based on the acquired data in respect of central compound model and response surface methodology. Table 5 shows the abundances of produced nanofibers on glassy slides observed using an optical microscope.

Table 5 shows the abundance data for the collected nanofiber based on SEM images using a number between 1 (the lowest) and 10 (the highest) nanofiber density. A second-degree polynomial equation fits to the experimental data for the prediction of response to the Selected zone based on the statistical analysis. The experimental design software provides coefficients of regression and ANOVA analysis results for response variables. The coefficients of functions and lack of fitness tests were used for determining the degree of precision of model. The coefficients explain the relation between the dependent and the independent variables. The R^2 value varies from zero to 1; the upper limit 1 means that the model considers all experimental data, and the zero value can be interpreted to mean the model is totally wrong. The prediction is considered outstanding when the R^2 value is more than 0.8. The test results for the examined models are shown in Table 8. As

can be seen, the second-degree polynomial model shows higher R^2 , calibrated R^2 , and estimated R^2 values, and lower standard deviation. Therefore, it indicates the greater fit on experimental data to help analyze experimental data and to find a full perspective on variable domain (Table 6).

The next step focuses on the variance calculation based on the reminders of standard deviation. If reminders stand in a straight line, then they follow standard deviation. In addition, the predicted quantities in contrast with real quantities should have a linear relation and consistent slope.

The effectiveness of parameters was studied based on fiber abundance quantity. The graph of decisive effects of factors consists of two vertical and horizontal axes. Vertical axis corresponds to response variable, while horizontal axis indicates factors.


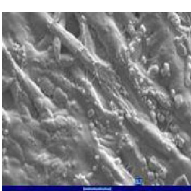


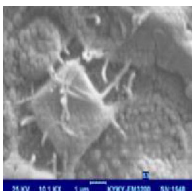

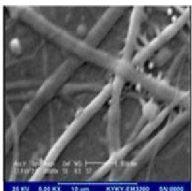
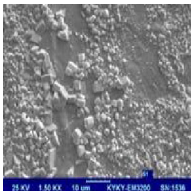
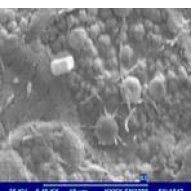
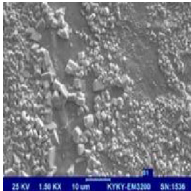
The lower slope change for the perturbation line predicts the lower influence on response variable. Figure 7 shows that the spinneret rotation (Sr), compared to two other factors, has smaller change of slope. It can be attributed to the lower influence of Sr on nanofiber abundance. However, the higher slope change corresponds to the voltage, which has a maximum effect on nanofiber abundance. The interaction graphs were used to show how the factors' interaction levels vary and their effects on response variable. If parallel lines appear between factors, then there is no remarkable interaction between the two factors. The blue color represents a region of the least nanofiber abundance, whereas red color indicates regions with the most nanofiber abundance. Moving from blue areas to red areas demonstrates higher nanofiber abundance. Figure 8 shows the interaction of Sr, and the distance between spinneret and collector (Sd) on nanofiber abundance. As can be seen, it is almost impossible to approach red areas, while rate and distance vary within the defined range of experimental design. It can be concluded that interaction of these two elements in nanofiber abundance is almost negligible (Fig. 8).

Figure 9 illustrates interaction between two factors: voltage and distance, on the abundance of nanofibers' production with needleless electrospinning. As can be seen in the graph, the higher the voltage the more the possibility, of reaching red areas, which illustrates far greater production of nanofibers. Of course, the distance should be less than 6 cm. It has to be considered that at the voltages less than 55 kV for all distances, there is almost no chance of producing nanofibers (Fig. 10).

Figure 11 shows the largest nanofiber abundances for the optimal quantities of spinning parameters including spinneret rate, distance, and voltage for producing nanofibers. It is worthy to note that the maximum abundance of nanofibers in the prescribed range of rate, distance, and



Table 5 Fiber abundance on glassy slide by verifying images of optical microscope

Set	condition		SEM	set	condition		SEM
1	Sr	5	 Abundance= 2	6	Sr	8.5	 Abundance= 2
	V	55			V	55	
	Sd	5			Sd	9	
2	Sr	8.5	 Abundance=3	7	Sr	5	 Abundance=6
	V	55			V	80	
	Sd	1			Sd	9	
3	Sr	12	 Abundance= 2	8	Sr	12	 Abundance= 4
	V	80			V	30	
	Sd	9			Sd	1	
4	Sr	8.5	 Abundance= 6	9	Sr	8.5	 Abundance= 1
	V	80			V	55	
	Sd	5			Sd	5	
5	Sr	8.5	 Abundance= 2	10	Sr	8.5	 Abundance= 1
	V	55			V	55	
	Sd	5			Sd	5	

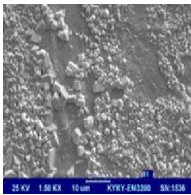
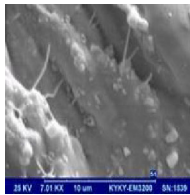
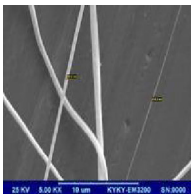


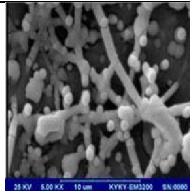
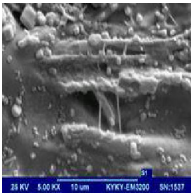
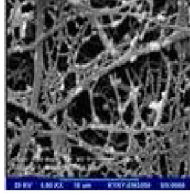
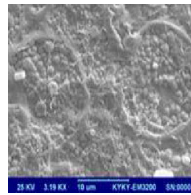
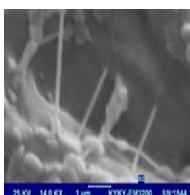
voltage does not provide the required density for practical application.

Therefore, the maximum abundance is unlikely to produce cellulosic nanofibers web useful for diverse applications in large scale. The main reason for poor production quality and quantity in large scale can be attributed to a few reasons related to the nature of spinning solution and

limitation in the electrospinning machine. The cellulosic chains have a high rigidity because of their powerful hydrogen bonds. Despite other needleless electrospinning frames which mostly use rotational rates greater than 1000 rpm for spinneret, the maximum speed of spinneret is 9 rpm, and as a consequence, the essential force and torque necessary to create primary turbulence and disturbance are



Table 5 continued

set	condition		SEM	set	condition		SEM
11	Sr	8.5	 Abundance= 1	16	Sr	12	 Abundance= 2
	V	55			V	55	
	Sd	5			Sr	5	
12	Sr	5	 Abundance= 5	17	Sr	8.5	 Abundance= 3
	V	30			V	55	
	Sd	9			Sd	5	
13	Sr	12	 Abundance= 3	18	Sr	12	 Abundance= 7
	V	30			V	80	
	Sd	9			Sd	1	
14	Sr	5	 Abundance= 3	19	Sr	5	 Abundance= 8
	V	30			V	80	
	Sd	1			Sd	1	
15	Sr	8.5	 Abundance= 2	20	Sr	8.5	 Abundance= 3
	V	30			V	55	
	Sd	5			Sd	5	

not significant, and the possibility of producing Taylor cone decreases. Despite the tremendous effort for collection of high-density nanofiber mat, all strategies led to non-homogenous low-density layer of nanofiber. Therefore, polyvinyl alcohol (PVA) is proposed as a electrospinning auxiliary polymer with desirable electrospinning specifications.

Polyvinyl alcohol as an auxiliary polymer

The PVA is used as a suitable auxiliary, low-cost polymer, easily soluble in water to facilitate the electrospinning process. It is a material with a biocompatible and biodegradable characteristics with efficient physical properties like hydrophilicity and ease of processing. The PVA



Table 6 Test results of fitting models

Standard deviation	R^2	Adjusted R^2	Predicted R^2	
1.3	0.6625	0.5992	0.3280	Linear
0.62	0.9524	0.9906	0.5402	Polynomial

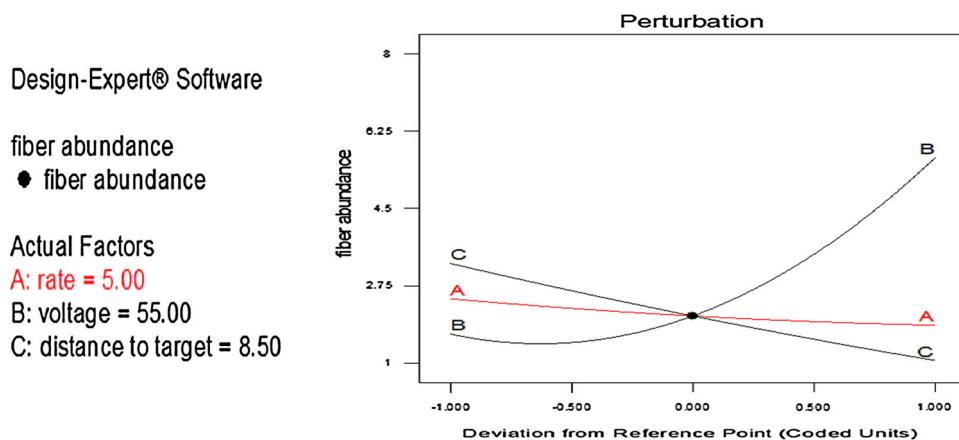
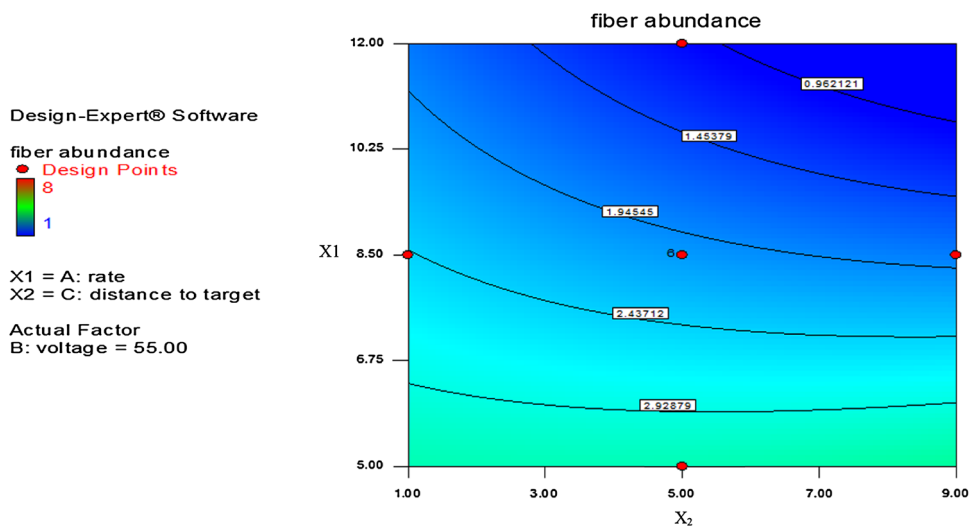
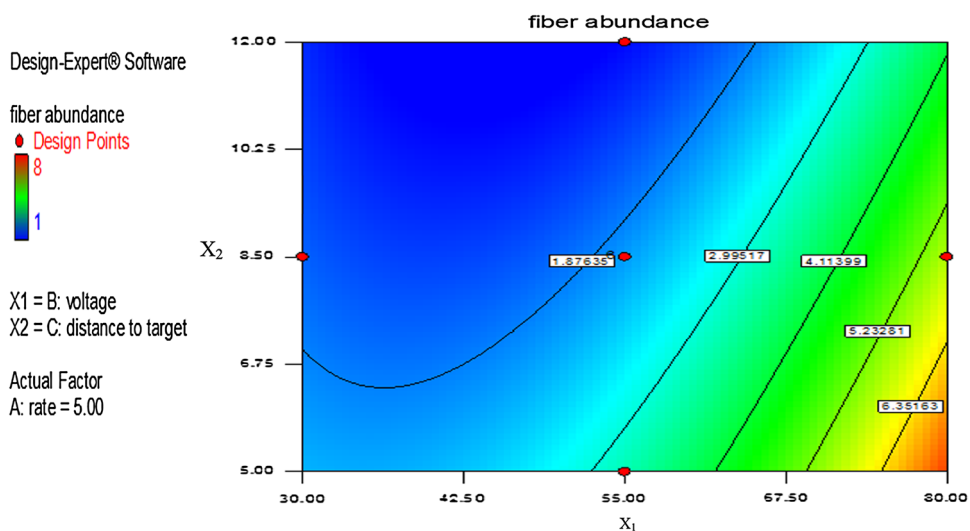
Fig. 7 The graph of decisive effects of factors**Fig. 8** Interaction between spinneret rotation and distance on nanofiber abundance**Fig. 9** The interaction between voltage and distance on nanofiber abundance

Fig. 10 The graph of interaction between voltage and spinneret rotation for nanofiber abundance

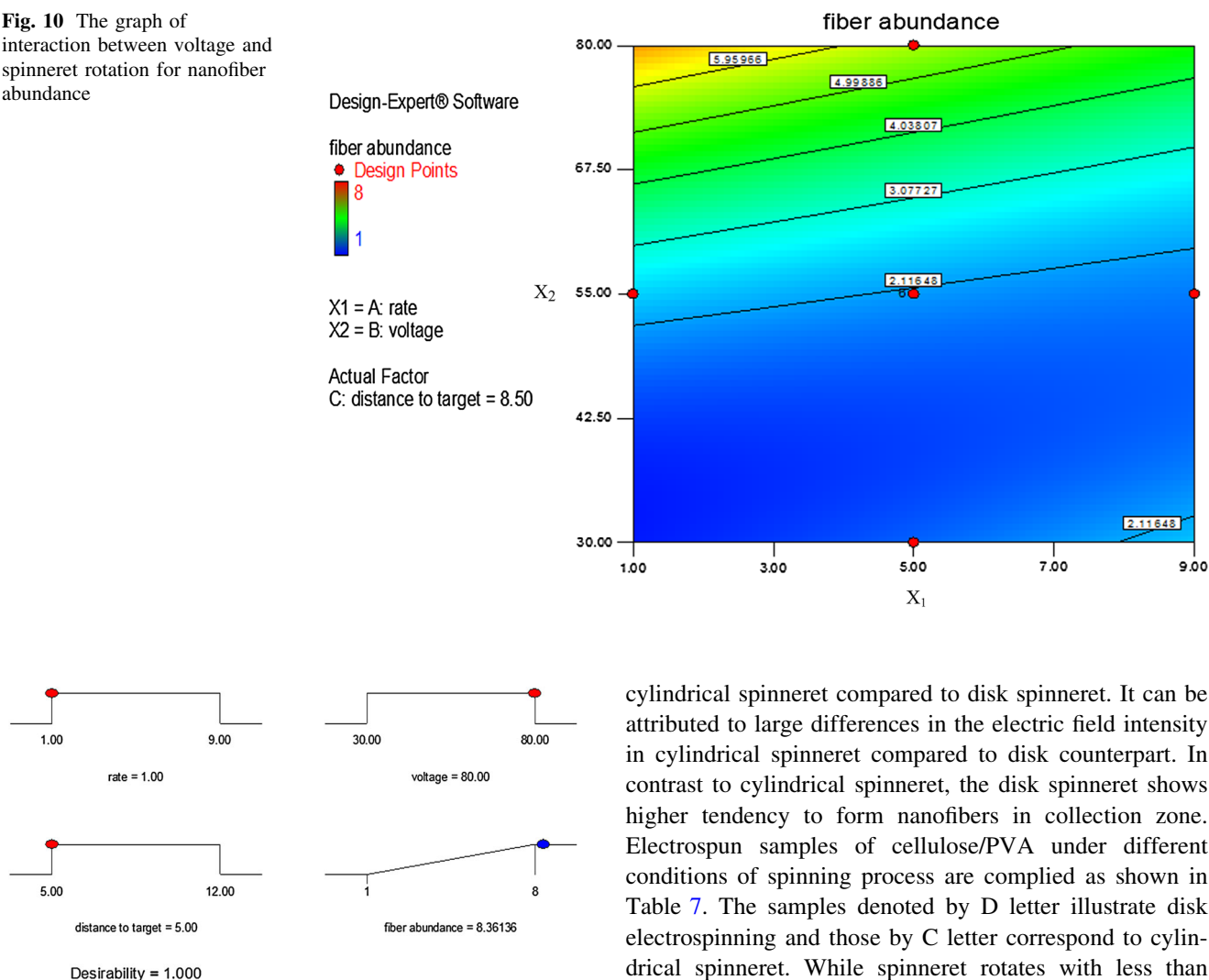


Fig. 11 The preferred quantity for spinneret rate, distance, and voltage for the highest abundance of nanofibers

addition to cellulose electrospinning solution leads to changes in electric properties, surface tension, and viscosity. Preliminary observations with optical microscope illustrated the lower possibility of producing nanofiber with

cylindrical spinneret compared to disk spinneret. It can be attributed to large differences in the electric field intensity in cylindrical spinneret compared to disk counterpart. In contrast to cylindrical spinneret, the disk spinneret shows higher tendency to form nanofibers in collection zone. Electrospun samples of cellulose/PVA under different conditions of spinning process are complied as shown in Table 7. The samples denoted by D letter illustrate disk electrospinning and those by C letter correspond to cylindrical spinneret. While spinneret rotates with less than 5 rpm, applying high voltage causes electrical discharge or spark between spinneret and collector because of charge accumulation in polymeric solution on the spinneret surface.

This occurs more prevalently in disk spinneret because of either intensive electric field or the thickness of the disk. Therefore, it is suggested to increase spinneret rotation rate until sparking initiation. On the other hand, the thermal

Table 7 Sample electrospinning of cellulose/polyvinyl alcohol

Temperature (°C)	Distance to collector (cm)	Voltage (kV)	Rate (rpm)	Sample
1 ± 40	10	1 ± 55	9	D1
30 ± 1	10	1 ± 55	9	D2
1 ± 40	10	1 ± 55	5	D3
1 ± 40	10	1 ± 40	9	D4
1 ± 40	5	40 ± 1	9	D5
1 ± 40	10	1 ± 35	5	D6
1 ± 40	5	1 ± 30	5	D7
1 ± 40	10	1 ± 60	9	C1



Table 8 Quantities of threshold for three superficial layers

Threshold	Quantity
1. Superficial layer	0.7358
2. Superficial and middle	0.4829
3. Middle and deep	0.2439

system is able to provide the maximum temperature of 45 °C. The higher the temperature, the more the decrease in surface tension. Therefore, it is extremely difficult to examine temperature effect during electrospinning process. Also, for distances smaller than 9–10 cm between spinneret and collector, it is not possible to apply voltage greater than 50 kV. It is mostly because of the inverse relation between the distance and the electric field. As a consequence, the working electric potential must not be set beyond the range of ± 50 kV. Table 8 shows that the decrease in distance naturally increases the applied voltage for the samples coded by D5 and D7. Figure 12 shows the SEM images of the as-prepared samples based on processing conditions given in Table 7.

Since the electrospun product for filter application needs higher thickness, longer duration of time is needed for nanofiber formation. Accordingly, the electrospinning process takes an average time between 45 and 60 min to pile up several layers of nanofibers. Therefore, a ribbon-

like morphology can be observed in Figs. 12 and 13 since solvent separation for surface layer of collected nanofibers is fairly insignificant on collector.

Zhang and his colleagues [54] postulate that semi-solid fibers rapidly discharge once they reach the target plate. However, when they are covered with other low conductivity layers, discharging process of bottom layers does not reach a proper completion. The remaining charge finally causes low-stretched nanofiber and higher fiber diameter for higher nanofiber layer thickness [54].

It was observed that sample D1 has a lower average diameter, and the cylindrical shape of nanofiber can be attributed to the efficiency of solvent separation. Compared with sample D1, The D2 sample shows higher average diameter and higher ribbon-like structure because of lower spinning temperature. In the meantime, the sample D3 shows higher average diameter compared to D1 with regard to lower spinneret rotation speed. While the spinneret rotation speed increases, the upward motion in polymeric solution also increases. This effect enables applying the high voltage, which leads to the stretching effect in the produced nanofibers. When the speed is low, stimulation and tension effect in solvent compared to higher speed is low, and it could apply further stretching at still higher voltages. As can be expected, the sample D4 shows the higher range of values of nanofiber diameter because of lower stretching tension in polymer streamline.

Fig. 12 SEM images of the samples prepared by the protocol: **a** D1 with average diameter of 89 ± 1 nm, **b** D2 with average diameter 139 ± 1 nm, **c** D3 with average diameter 154 ± 1 nm, **d** D4 with average diameter 158 ± 1 nm

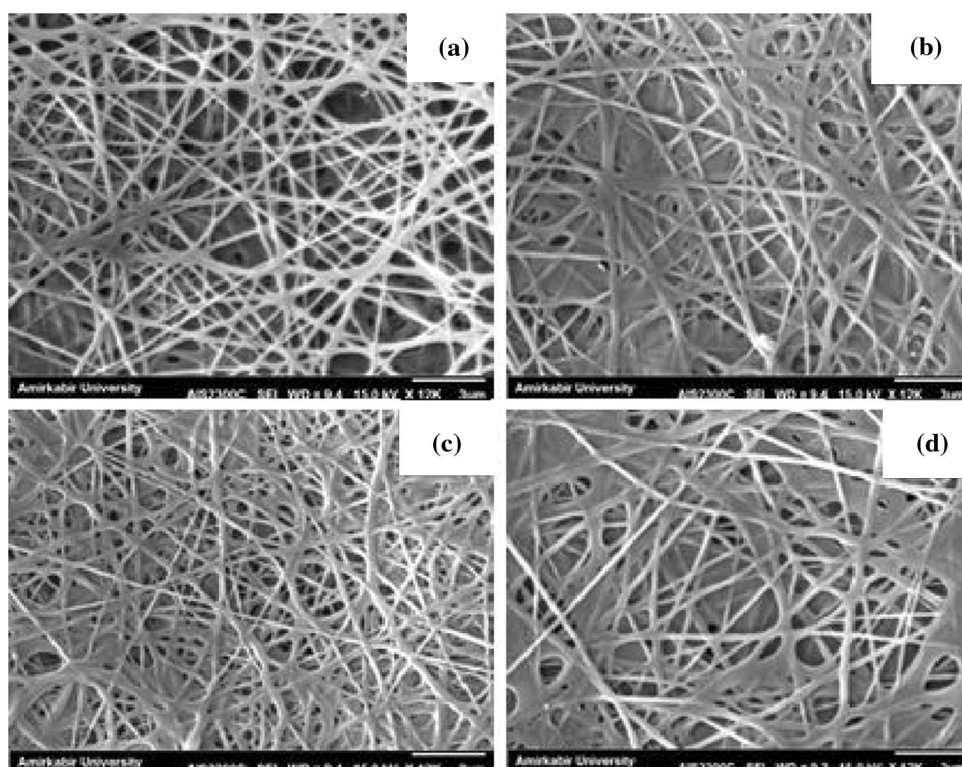
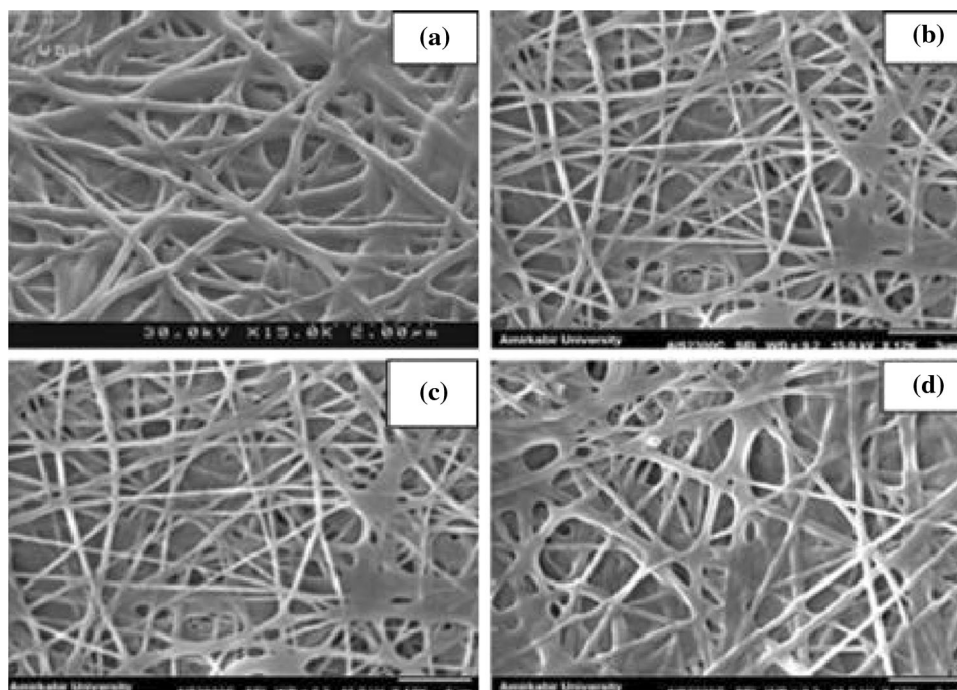


Fig. 13 SEM images of the samples prepared by the protocols **a** D5 with average diameter of 123 ± 1 nm, **b** D6 with average diameter 191 ± 1 nm, **c** D7 with average diameter 184 ± 1 nm, **d** C1 with average diameter 237 ± 1 nm



Similarly, the sample D5 shows higher average diameter for smaller distance, and therefore there is no room for sufficient stretching and solvent separation. As was previously mentioned, at the distances less than 10 cm, it is impossible to apply voltages higher than 50 kV. Hence, the shorter the distances it was, the less the voltage that was needed. It is observed that in the samples D6 and D7 prepared at 5 rpm speeds, regardless of other parameters, the average diameters of nanofibers are higher compared to those of other electrospun samples with disk spinneret. The C1 sample is the only one that was done by cylindrical spinneret. In this sample, because of electric discharge during electrospinning, there was no possibility for spinning at 9 rpm—although, in this case little solvent evaporation could be seen; however, with regard to weakness of spinneret electric field, the maximum voltage is applicable. According to these interpretations, by considering the electrospinning device limitations, the speed, voltage, distance, and temperature, respectively, have values of 9 rpm, 55 kV, 10 cm, and 41 °C for the most homogenous sample with the lowest average diameter in D1 sample.

The porosity analysis

Based on the SEM images, the Matlab software utilized for measuring the porosity of multilayer nanofiber. For this purpose, in the primary step, the image shifts to gray scale which includes black, gray, and white ranges of

colors. Then, the images transferred to double area which is necessary for determining a threshold based on previous investigations. In fact, three thresholds' limits need to be defined. Each threshold distinctively penetrates into a layer and illustrates the double image at that depth. According to black and white nature of double images, analysis is carried out on these figures in which the ratio of pores' pixels to total number of pixels is defined as the porosity. The formula (1) indicates the percentage of porosity based on the ratio of pixel of pores to total number of pixels.

$$\text{porosity} = \frac{\text{pixel}_{\text{pore}}}{\text{pixel}_{\text{total}}} \times 100 \quad (1)$$

Picture analysis by MATLAB software produces Histogram of images which defines intensity of white through black colors based on pixel distribution (Fig. 14).

Using average and standard deviation of layer Histogram, the quantities of thresholds for three superficial layers are calculated through formulas given below

$$\text{Threshold1: } (\mu + \sigma)/255 \quad (2)$$

$$\text{Threshold2: } (\mu)/255 \quad (3)$$

$$\text{Threshold3: } (\mu - \sigma)/255 \quad (4)$$

Threshold number enables the images to switch from grayscale to double mode in which each pixel of image can only be colored black or white. Further calculation is carried out according to black and white points.

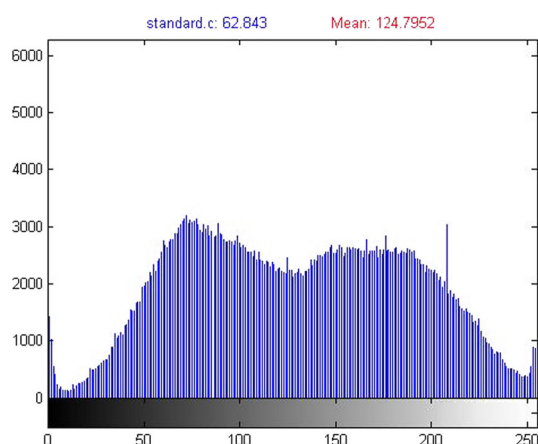


Fig. 14 Real image Histogram of D1 sample

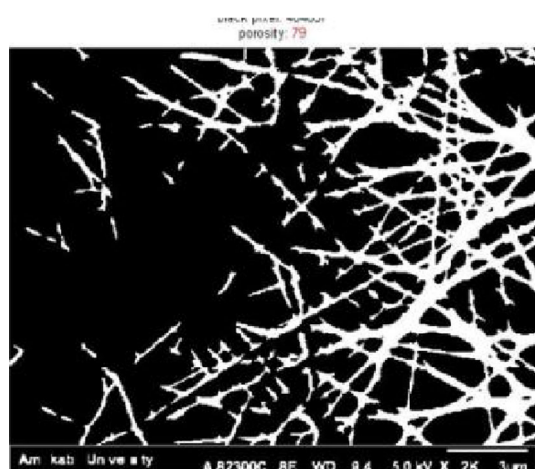
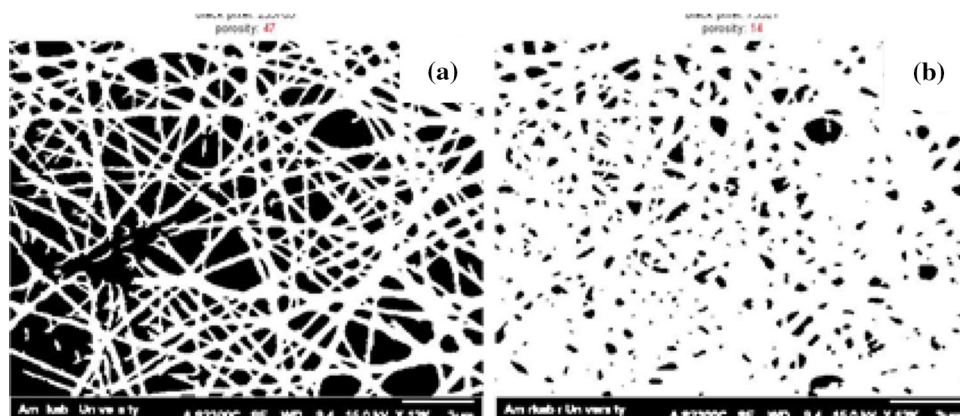


Fig. 15 Double-mode images based on threshold level 1 with 79 % porosity

As can be observed, the higher the threshold number, the more nanofibers turn to the white color. As a matter of fact, the lower number of layers is also under consideration (Figs. 15, 16). Paying attention to the formula of

Fig. 16 **a** Double-mode images based on threshold level 1 with 47 % porosity, **b** based on threshold level 3 with 14 % porosity



calculating porosity which is the ratio of black pixels to total pixels reveals that the porosity is lower for early layer. Finally, average porosity from every three layers is clarified as a total porosity. The above method was also used for other samples as shown in Table 9.

Air permeability measurement

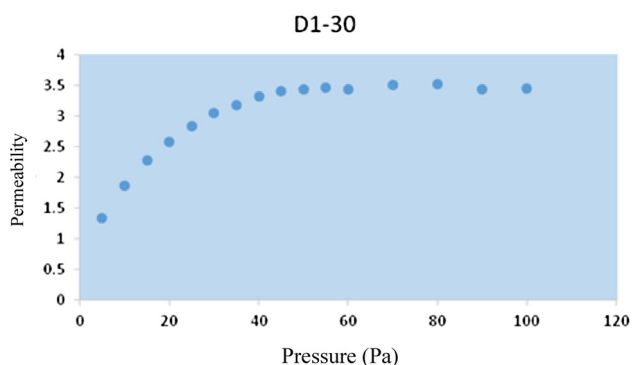
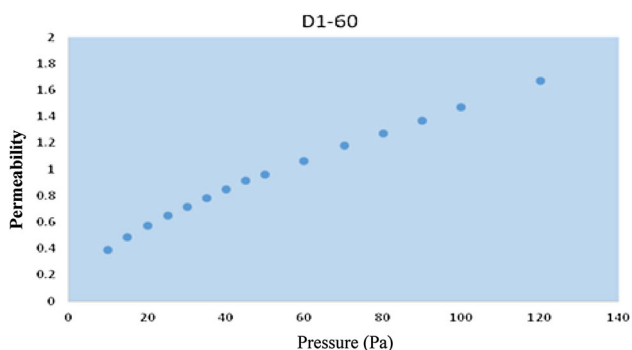
Porosity and air permeability are vital properties in some end-use applications such as filtration, thermal insulation, and fluid barriers. The various permeability tests to evaluate textiles and textile materials have been applied in practice in the industry for many years, and determinations of permeability and porosity have long been subjects of interest in this field. Previous studies investigated the relationship between air permeability and structural characteristics of nonwoven fabrics, such as fabric weight, thickness, density, and fiber diameter [55]. It has generally been demonstrated that air permeability decreases as thickness, weight, or fabric density increases. Using nanofiber in filtration industry is similarly concerned with physical properties of nanoweb filter. In the meantime, the lower strength of nanofibers is a limitation against reproducible air permeability test. Therefore, it is only possible for samples which were electrospun under the conditions mentioned for D1 sample. Effect of electrospinning duration on permeability value was investigated by considering two time ranges of 30 min (D1-30) and 60 min (D1-60) for electrospun samples. Figures 17 and 18 show the permeability ($\text{cm}^3/\text{cm}^2/\text{s}$) data as a function of applied pressures (Pa). Table 10 provides the information regarding to the pressures corresponding to maximum and minimum permeabilities.

The permeability variation clearly demonstrates the inverse functionality of permeability versus electrospinning time. This finding is in agreement with the observation reported previously by Gorji and his coworkers on Polyurethane nanofibers. It was shown that with the increasing



Table 9 Percentages of porosity for collected samples

Porosity (%)	Sample
46	D1
46	D2
46	D3
47	D4
47	D5
47	D6
46	D7
48	C1

**Fig. 17** Permeability graph for D1-30 samples**Fig. 18** Permeability graph for D1-60 samples**Table 10** Pressures at maximum and minimum of Permeability

Pressure at maximum permeability (Pa)	Pressure at minimum permeability (Pa)	Sample
100	5	D1-30
120	10	D1-60

time period of electrospinning and thickness of the nanolayer, the amount of air permeability decreases which has a nonlinear relation with layer's thickness [56].

Conclusions

Cellulose extracted from rice straw as a biocompatible, abundant, inexpensive, and renewable polymer was used as raw material for production of cellulose nanofibers. The high swelling capacity of the cellulose samples prepared from rice straw promotes the water as a biocompatible, abundant, and cheap solvent. The strong hydrogen bonds in cellulose structure, the high surface tension, and low conductivity conduct the research roadmap toward using the appropriate quantities of surfactant and lithium chloride salt. By measuring the surface tension, viscosity, and conductivity of the prepared samples, the cellulose solution of 0.63 % w/w containing 1 % w/w lithium chloride salt and proper value of surfactant was chosen as suitable for the electrospinning process. The low flexibility of the cellulose structure resulted in frustrating results for the production of nanofiber. As a result, a polymer like PVA used as an auxiliary polymer to provide easier condition for electrospinning process. The samples of 0.63 % w/w with weight ratio of 60:40 (cellulose to PVA) was chosen for the electrospinning process carried out at different voltages, speed, distance, and temperature. The electrospun nanofiber samples collected with rotation rate, voltage, distance, and temperature, respectively, being set to 9 rpm, 55 kV, 10 cm, and 40 °C show a mean diameter of 89 ± 1 nm less than the average diameter compared to those of other samples. Measurement of the porosity of electrospun samples shows high porosity for the collected sample. The air permeability tests for samples with the highest mechanical strengths at different test durations of 30 and 60 min at a pressure of 100 Pa, show the average values, respectively, of 3.4 and $1.75 \text{ cm}^3/\text{cm}^2/\text{s}$.

Acknowledgments The authors would like to express their sincere appreciation and thanks to Iran Nanotechnology Initiative Council, the University of Guilan and Guilan Science Technology Park (GSTP) for their financial and technical supports.

Open Access This article is distributed under the terms of the Creative Commons Attribution 4.0 International License (<http://creativecommons.org/licenses/by/4.0/>), which permits unrestricted use, distribution, and reproduction in any medium, provided you give appropriate credit to the original author(s) and the source, provide a link to the Creative Commons license, and indicate if changes were made.

References

1. Alemdar A, Sain M (2008) Isolation and characterization of nanofibres from agricultural residues-wheat straw and soyhulls. *Bioresour Technol* 99:1664–1971
2. Alemdar A, Sain M (2008) Biocomposites from wheat straw nanofibers: morphology, thermal and mechanical properties. *Compos Sci Technol* 68(2):557–565



3. Alila S, Besbes I, Vilar MR, Mutjé P, Boufi S (2013) Non-woody plants as raw materials for production of microfibrillated cellulose (MFC): a comparative study. *Ind Crops Prod* 41:250–259
4. Besbes I, Vilar MR, Boufi S (2011) Nanofibrillated cellulose from Alfa, Eucalyptus and Pine fibres: preparation, characteristics and reinforcing potential. *Carbohydr Polym* 86(3):1198–1206
5. Zhang J, Guo R-B, Qiu Y-L, Qiao J-T, Yuan X-Z, Shi X-S, Wang C-S (2015) Combined pretreatment using ozonolysis and ball milling to improve enzymatic saccharification of corn straw. *Bioresour Technol* 179:444–451
6. Zhu S, Huang W, Huang W, Wang K, Chen Q, Wu Y (2015) Coproduction of xylose, lignosulfonate and ethanol from wheat straw. *Bioresour Technol* 185:234–239
7. Kurokuchi Y, Sato M (2015) Properties of binderless board made from rice straw: the morphological effect of particles. *Ind Crops Prod* 69:55–59
8. Miao Q, Tang Y, Xu J, Liu X, Xiao L, Chen Q (2013) Activated carbon prepared from soybean straw for phenol adsorption. *J Taiwan Inst Chem Eng* 44(3):458–465
9. Cherian BM, Leão AL, de Souza SF, Thomas S, Pothan LA, Kottaisamy M (2010) Isolation of nanocellulose from pineapple leaf fibres by steam explosion. *Carbohydr Polym* 81(3):720–725
10. Reddy N, Yang Y (2009) Natural cellulose fibers from soybean straw. *Bioresour Technol* 100(14):3593–3598
11. Abe K, Yano H (2011) Formation of hydrogels from cellulose nanofibers. *Carbohydr Polym* 85(4):733–737
12. Abdul Khalil HPS, Bhat AH, Ireana Yusra AF (2012) Green composites from sustainable cellulose nanofibrils: a review. *Carbohydr Polym* 87(2):963–979
13. Liu CF, R-CS “Cellulose” chapter 5, pp 131–167
14. Niu K, Chen P, Zhang X, Tan W-S (2009) Enhanced enzymatic hydrolysis of rice straw pretreated by alkali assisted with photocatalysis technology. *J Chem Technol Biotechnol* 84(8):1240–1245
15. Ranjan A, Moholkar VS (2013) Comparative study of various pretreatment techniques for rice straw saccharification for the production of alcoholic biofuels. *Fuel* 112:567–571
16. Binod P, Sindhu R, Singhania RR, Vikram S, Devi L, Nagalakshmi S, Kurien N, Sukumaran RK, Pandey A (2010) Bioethanol production from rice straw: an overview. *Bioresour Technol* 101(13):4767–4774
17. Lu P, Hsieh Y-L (2012) Preparation and characterization of cellulose nanocrystals from rice straw. *Carbohydr Polym* 87(1):564–573
18. Karimi K, Kheradmandinia S, Taherzadeh MJ (2006) Conversion of rice straw to sugars by dilute-acid hydrolysis. *Biomass Bioenergy* 30(3):247–253
19. Zimmermann T, Bordeanu N, Strub E (2010) Properties of nanofibrillated cellulose from different raw materials and its reinforcement potential. *Carbohydr Polym* 79:1086–1093
20. De Moraes Teixeira E, Carolina Corrêa A, Manzoli A, Lima Leite F, De Oliveira C, Mattoso L (2010) Cellulose nanofibers from white and naturally colored cotton fibers. *Cellulose* 17:595–606
21. Klemm D, Schumann D, Kramer F, Heßler N, Koth D, Sultanova B (2009) Nanocellulose materials-different cellulose, different functionality. *Macromol Symp* 280:60–71
22. Ziabari M, Mottaghitalab V, Haghi AK (2008) Simulated image of electrospun nonwoven web of PVA and corresponding nanofiber diameter distribution. *Korean J Chem Eng* 25(4):919–922
23. Xu S, Zhang J, He A, Li J, Zhang H, Han CC (2008) Electrospinning of native cellulose from nonvolatile solvent system. *Polymer* 49(12):2911–2917
24. Ahn Y, Hu DH, Hong JH, Lee SH, Kim HJ, Kim H (2012) Effect of co-solvent on the spinnability and properties of electrospun cellulose nanofiber. *Carbohydr Polym* 89(2):340–345
25. Ahn Y, Hu D-H, Hong JH, Lee SH, Kim HJ, Kim H (2012) Effect of co-solvent on the spinnability and properties of electrospun cellulose nanofiber. *Carbohydr Polym* 89(2):340–345
26. Mottaghitalab V, Farjad M (2013) Electrospun cellulosic structure nanofiber based on rice straw. *J Polym Eng* 33(9):857–873
27. Jia B, Zhou J, Zhang L (2011) Electrospun nano-fiber mats containing cationic cellulose derivatives and poly (vinyl alcohol) with antibacterial activity. *Carbohydr Res* 346:1337–1341
28. Sadrahani M, Hoseini SA, Mottaghitalab V, Haghi AK (2011) PAN monofilament in nanoscale: a novel approach. *E-Polymers*
29. Mahdih ZM, Mottaghitalab V, Piri N, Haghi AK (2012) Conductive chitosan/multi walled carbon nanotubes electrospun nanofiber feasibility. *Korean J Chem Eng* 29(1):111–119
30. Ziabari M, Mottaghitalab V, Haghi AK (2010) A new approach for optimization of electrospun nanofiber formation process. *Korean J Chem Eng* 27(1):340–354
31. Luo CJ, Stoyanov SD, Stride E, Pelan E, Edirisinghe M (2012) Electrospinning versus fibre production methods: from specifics to technological convergence. *Chem Soc Rev* 41:4708–4735
32. Wang X, Niu H, Wang X, Lin T (2012) Needleless electrospinning of uniform nanofibers using spiral coil spinnerets. *J Nanomater* 2012:3
33. Niu H, Lin T (2012) Fiber generators in needleless electrospinning. *J Nanomater* 2012:12
34. Simm W, Gosling C, Bonart R, Falkai BV (1979) Fibre fleece of electrostatically spun fibres and methods of making same
35. Jirsak O, Sanetrik F, Lukas D, Kotek V, Martinova L, Chaloupek J (2009) A method of nanofibres production from a polymer solution using electrostatic spinning and a device for carrying out the method
36. Niu H, Lin T, Wang X (2009) Needleless electrospinning. I. A comparison of cylinder and disk nozzles. *J Appl Polym Sci* 114(6):3524–3530
37. Yarin A, Zussman E (2004) Upward needleless electrospinning of multiple nanofibers. *Polymer* 45(9):2977–2980
38. Liu Y, He J-H, Yu J-Y (2008) Bubble-electrospinning: a novel method for making nanofibers. *J Phys: Conference Series*. IOP Publishing
39. Gangwal S, Wright M (2013). Nanofibres: new scalable technology platform for producing polymeric nanofibres. *Filtration + Separation* 50(2):30–33
40. Anitha S, Brabu B, John Thiruvadigal D, Gopalakrishnan C, Natarajan TS (2012) Optical, bactericidal and water repellent properties of electrospun nano-composite membranes of cellulose acetate and ZnO Original Research Article. *Carbohydr Polym* 87(2):1065–1072
41. Rosu C, Manaila Maximean D, Kundu S, Almeida PL, Danila O (2011) Perspectives on the electrically induced properties of electrospun cellulose/liquid crystal devices. *J Electrostat* 69(6):623–630
42. Huang C, Soenen SJ, Ev Gulck, Vanham G, Rejman J, Calenbergh SV, Vervaeke C, Coenye T, Verstraeten H, Temmerman M, Demeester J, De Smedt SC (2012) Electrospun cellulose acetate phthalate fibers for semen induced anti-HIV vaginal drug delivery. *Biomaterials* 33(3):962–969
43. Castillo-Ortega MM, Nájera-Luna A, Rodríguez-Félix DE, Encinas JC, Rodríguez-Félix F, Romero J, Herrera-Franco PJ (2011) Preparation, characterization and release of amoxicillin from cellulose acetate and poly(vinyl pyrrolidone) coaxial electrospun fibrous membranes. *Mater Sci Eng C* 31(8):1772–1778
44. Barhate R, Ramakrishna S (2007) Nanofibrous filtering media: filtration problems and solutions from tiny materials. *J Membr Sci* 296(1):1–8



45. Tan S, Huang X, Wu B (2007) Some fascinating phenomena in electrospinning processes and applications of electrospun nanofibers. *Polym Int* 56(11):1330–1339
46. Graham K, Ouyang M, Raether T, Grafe T, McDonald B, Knauf P (12 April 2002) Fifteenth annual technical conference & expo of the American Filtration & Separations Society. Galveston
47. Ngiam M, Ramakrishna S, Raghunath M, Chan CK (2007) Nanofiber patent landscape. *Recent Pat Nanotechnol* 1(2):137–144
48. Lee B-B, Ravindra P, Chan E-S (2009) New drop weight analysis for surface tension determination of liquids. *Colloids Surf A* 332(2):112–120
49. Ghasemi-Mobarakeh L, Semnani D, Morshed M (2007) A novel method for porosity measurement of various surface layers of nanofibers mat using image analysis for tissue engineering applications. *J Appl Polym Sci* 106(4):2536–2542
50. Abuzade RA, Zadhoush A, Gharehaghaji AA (2012) Air permeability of electrospun polyacrylonitrile nanoweb. *J Appl Polym Sci* 126(1):232–243
51. Bhardwaj N, Kundu SC (2010) Electrospinning: a fascinating fiber fabrication technique. *Biotechnol Adv* 28(3):325–347
52. Liu D, Chen X, Yue Y, Chen M, Wu Q (2011) Structure and rheology of nanocrystalline cellulose. *Carbohydr Polym* 84(1):316–322
53. Angammana CJ, Jayaram SH (2011) Analysis of the effects of solution conductivity on electrospinning process and fiber morphology. *IEEE Trans Industry Appl* 47(3):1109–1117
54. Zhang Q, Welch J, Park H, Wu C-Y, Sigmund W, Marijnissen J (2010) Improvement in nanofiber filtration by multiple thin layers of nanofiber mats. *J Aerosol Sci* 41(2):230–236
55. Dent R (1976) The air permeability of nonwoven fabrics. *J Text Inst* 46(6):220–224
56. Gorji M, Jeddi A, Gharehaghaji A (2012) Fabrication and characterization of polyurethane electrospun nanofiber membranes for protective clothing applications. *J Appl Polym Sci* 125(5):4135–4141

